Deepak Jain*, Abhijit Mukherjee and Tarun Kumar Bera

A novel characterization method of fiber reinforced polymers with clustered microstructures for time dependent mass transfer

https://doi.org/10.1515/secm-2016-0063
Received March 1, 2016; accepted September 4, 2017; previously published online November 27, 2017

Abstract: Some variation in the topological distribution of fibers inside the matrix phase of fiber reinforced polymers (FRP) is inevitable. Such irregularities can accelerate moisture diffusion and adversely affect the life of FRP. This paper presents a hierarchical technique for characterization of clustered microstructures and their transient moisture diffusion response. The clustering descriptors are derived for different fiber volume fractions (dilute to dense) for the quantitative definition of a given fiber matrix architecture. The metrics are normalized to remove dependence on volume fraction. The microstructures are analyzed for Fickian moisture diffusion. Suggested descriptors show a good correlation with transient diffusion response in relation to saturation time. The results can be used to predict the time-dependent moisture diffusion response of FRPs for any given fiber volume fraction.

Keywords: FRP composites; mass diffusion; statistical characterization; structure property relationship.

1 Introduction

Present-day manufacturing techniques involve the use of sophisticated and automated equipment to manufacture fiber reinforced polymer (FRP) structures. However, the composites are not always perfectly manufactured and processing conditions can easily introduce typical defects. The defects such as accumulation of voids, air pockets, misplaced fibers, and resin rich pockets are inevitable [1]. Figure 1 illustrates a typical field of microstructural fiber distribution [2]. The micrograph represents the actual as-manufactured specimen. Lack of manufacturing control resulted in the formation of resin rich zones finally resulting in variability of bulk properties.

Amidst these defects, the clustered microstructures are often used for quantitative analysis of physical property relationship in composites when subjected to elastic [3, 4], thermal [5], mass diffusion [6–8], and electric [9] fields. The investigation of structure-property relationships requires close capture of several geometry attributes such as clusters locations, cluster strength, and inter- and intra-cluster interaction of inclusions. Most of the geometric characterization procedures involve data-mining measures for the distribution of reinforcements that grade the geometric information into numbers. Several criteria viz. Hill condition, probability density function, pair distribution function, and nearest neighbor distance have been suggested to determine the minimal statistical equivalent size of representative volume element (RVE) for the characterization the geometry [10, 11]. These methods have extensively been used in the past by many researchers. In this work we use the hierarchical data mining technique to pair the fiber reinforcements. A new descriptor to statistically characterize different fiber volume fraction has been suggested. Unlike most of the statistical techniques, this method can generate the clusters both in agglomerative (bottom-up) and divisive (top-down) manner. To the author's knowledge no studies have yet been undertaken for the statistical characterization of composite microstructures using the hierarchical clustering technique.

2 Cluster identification in FRPs

To characterize a microstructure, it is necessary to identify the physical clusters. Any given fiber matrix arrangement can be partitioned based on the fiber density. This can be done by extracting the microstructural topological information of a given random arrangement. In this work, the hierarchical approach of partitioning has been used to identify the clustering of a given fiber matrix arrangement and identification of clusters inside FRPs. This approach is also

***Corresponding author: Deepak Jain,** Mechanical Engineering Department, Thapar University, Patiala – 147004, India, Phone: +91-783-784-1951, e-mail: deepak.jain@thapar.edu
Abhijit Mukherjee: Department of Civil Engineering, Curtin University, Bentley 6102, WA, Australia
Tarun Kumar Bera: Mechanical Engineering Department, Thapar University, Patiala – 147004, India

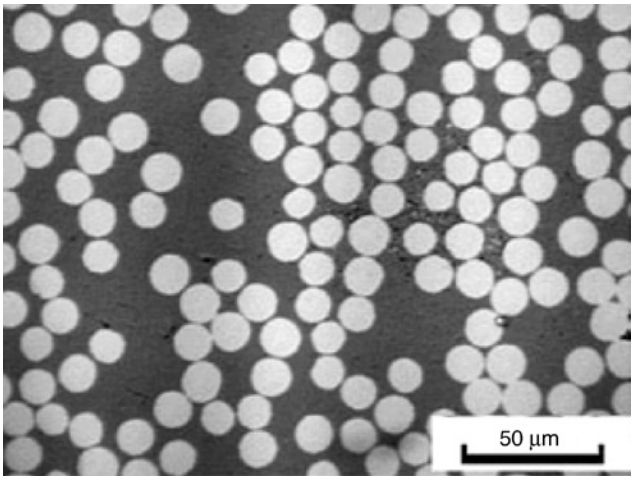

Figure 1: A typical fiber distribution microstructural field [2].

referred to as "inconsistency method". Further normalization is done to compare the effective clustering index of different fiber volume fraction (*Vf*) levels. Figures 2 and 3 show the example geometries used to illustrate this method. Figure 1 shows a "ring arrangement", and Figure 2 shows a "zoned arrangement". Two different clustering techniques (hierarchical and K-means method) have been used to identify the clusters in both the arrangements. On comparing the set of clusters, it can be observed that hierarchical approach yielded well-separated clusters. It was noticed that the method of hierarchical clustering successfully partitioned the ring arrangement into two and into three different clusters. Therefore, this technique has been used in the rest of this work to develop a novel clustering descriptor and to characterize the microstructures.

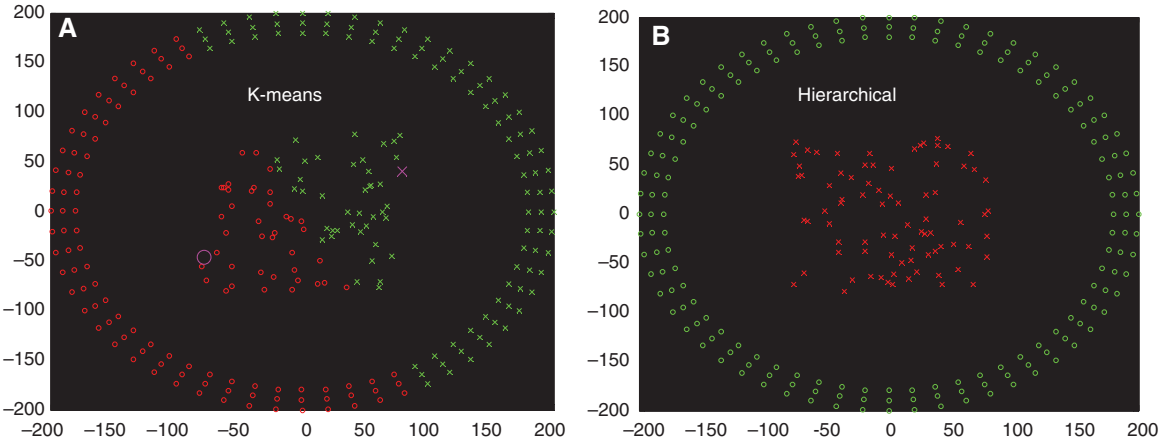

Figure 2: Clustering for ring arrangement by (A) K-means clustering technique and (B) hierarchical approach.

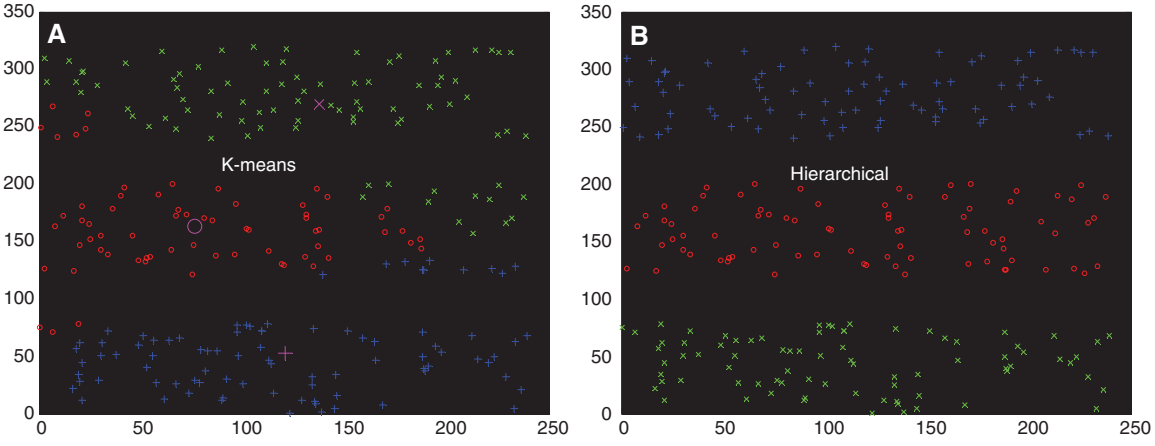

Figure 3: Clustering of zoned arrangement by (A) K-means and (B) hierarchical clustering approaches.

2.1 Hierarchical clustering – associated metrics

This section explains the hierarchical method of clustering. A cluster tree is initially formed by joining two objects at a time. Figure 4 shows a dendrogram generated through hierarchical clustering for the zoned arrangement shown in Figure 3. It is formed by joining two distinct hierarchy objects at a time. The procedure is repeated until all the objects are joined to the tree. Three distinct regions can be observed at the bottom. These regions represent the indices of three distinct clusters.

The object indices are shown along the X axis. The height along the Y axis indicates the straight line Euclidean distance between the two objects. The graph is based on the cohesion and separation between different objects. This cohesion and separation can be measured statistically through the height that indicates the average distance between the individual objects or clusters that contain these objects. The links at the same height exhibit a higher consistency. It indicates that the distance between the objects which are already under a link are approximately the same as the distance of the new objects being joined under this link. On the other hand, a higher difference in the height of the joined links is indicative of a larger distance between the joined objects. Such a link is considered inconsistent with respect to the links below it. In the current work, the consistency of each link with respect to the links below is represented by a quantified statistical measure termed as "inconsistency coefficient (Ψ)".

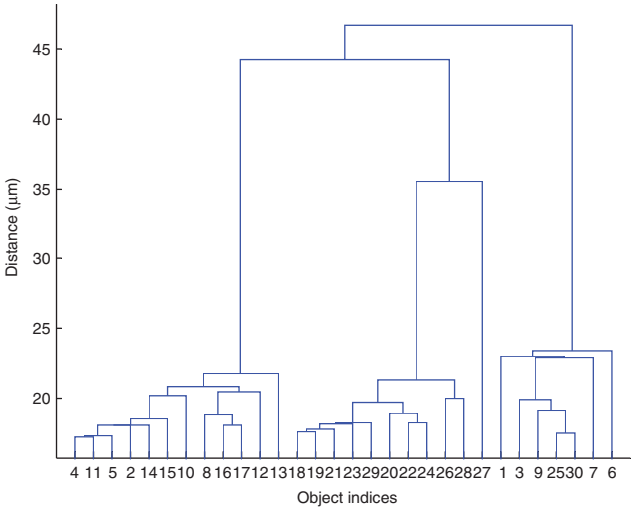

Figure 4: Hierarchical cluster tree (dendrogram) for zoned arrangement.

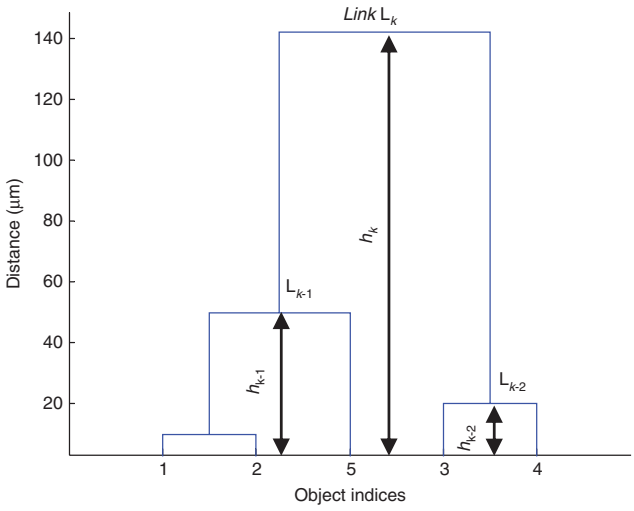

Figure 5: Representation of the height and link along a dendrogram.

Figure 5 shows an example where a hierarchical link L_k is formed by joining link L_{k-1} and L_{k-2}.

The inconsistency coefficient of the link L_K is normalized by standard deviation. It is evaluated according to the following relationship:

$$\Psi_k = \frac{h_k - h_m}{\sigma}. \tag{1}$$

Here h_k is the link height of link K. h_m is the mean height of the link L_K and two other links which are immediate to it, i.e. link L_{K-1} and L_K. The expression 2σ is the standard deviation of the heights of all three links. The mean height is calculated according to following relationship:

$$h_m = \frac{\sum_{i=0}^{n-1} h_{k-i}}{n}. \tag{2}$$

Here n is the number of links included in calculation. In the cluster tree, any object at the bottom having no objects below it is called "leaf node". The leaf nodes have "*zero*" inconsistency coefficient. The inconsistency coefficient of the links in the cluster tree is used to identify the any abrupt change in the similarity of the objects to partition them and identify the new clusters. The usage of this procedure is further explained by an example given in Appendix A.

2.2 Volume fraction (*Vf*) and inconsistency metric relationships

The random arrangement of fibers in matrix is considered for this analysis. The microstructures of variable

fiber volume fraction (*Vf*) are considered for the geometric characterization.

Figure 6 shows the range of fiber matrix configurations with fiber volume fraction from lean to dense (0.1–0.9). The threshold fiber packing limit is at a fiber volume fraction of *Vf* ~0.9 (bee honeycomb).

An increase in volume fraction resulting in development of "hexagonal cells" at higher volume fractions is shown in Figure 7. Any arbitrary model of a given volume fraction can be calibrated and compared against this "bee honeycomb" arrangement to determine its clustering level.

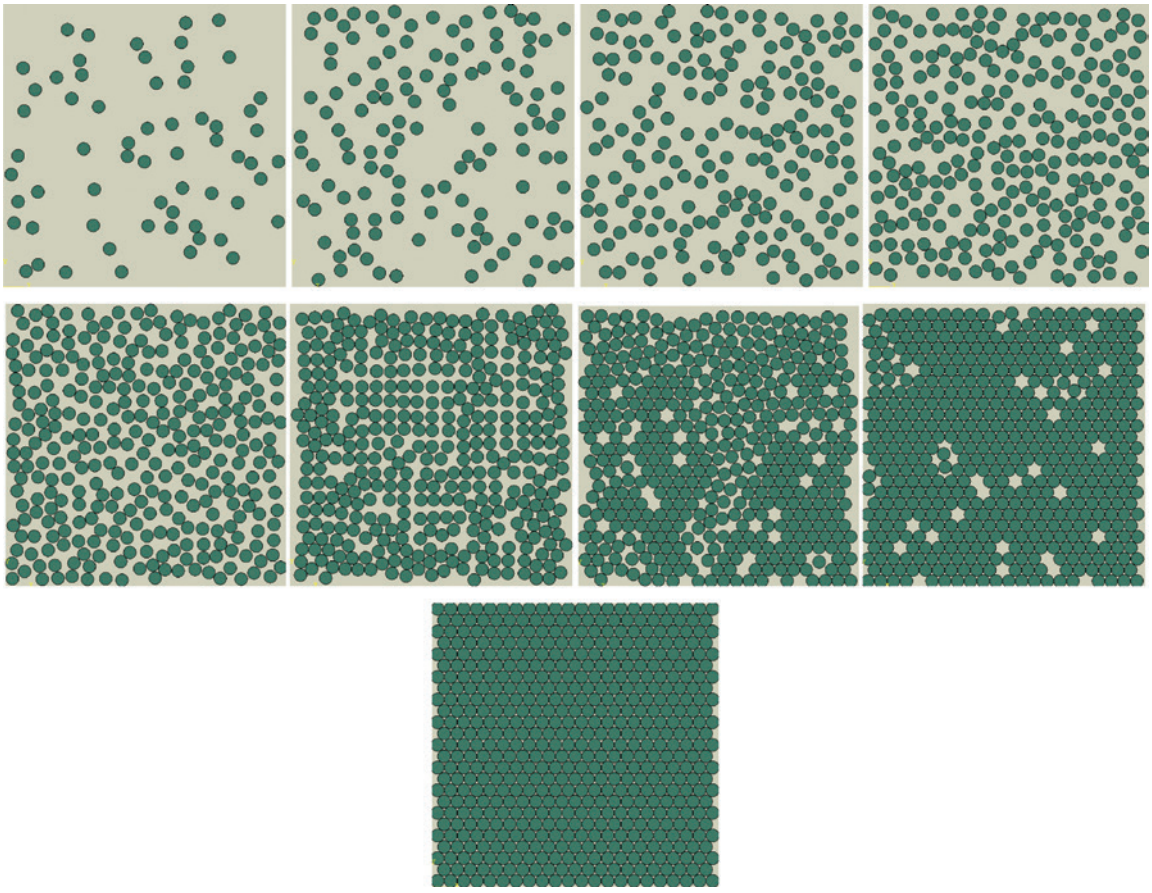

Figure 6: Images of different volume fractions 0.1, 0.2, 0.3, 0.4, 0.5, 0.60, 0.7, 0.8 and 0.9072 (bee honeycomb).

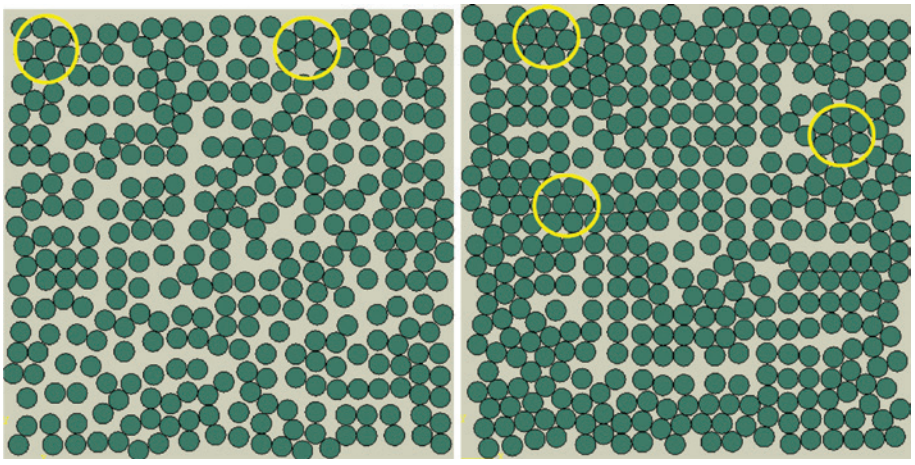

Figure 7: Development of hexagonal cells with the higher volume fractions.

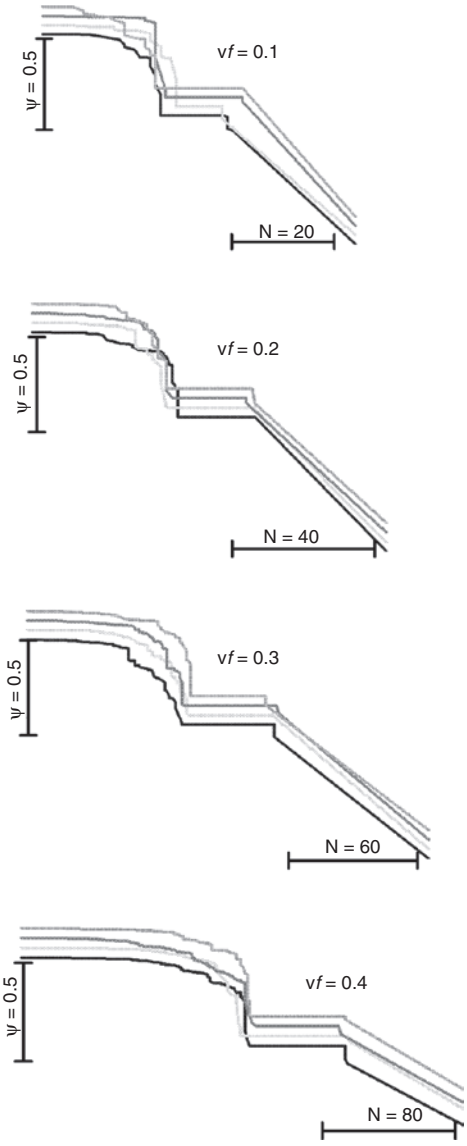

Figure 8: Scale plot of generated clusters count (N) vs. inconsistency coefficient (Ψ) for (A) $vf = 0.1$, (B) $vf = 0.2$, (C) $vf = 0.3$ and (D) $vf = 0.4$. (Curves are nudged by 0.05 unit along Y axis to prevent the overlap).

Figure 8 shows the scale plots between input inconsistency coefficients and corresponding cluster count. Different samples were taken for volume fraction ranging 0.1–0.9 inside a randomly seeded square of size 400 μm × 400 μm. All four graphs exhibit similar variation of clustering coefficient (Ψ) for all the sample models.

Figure 9 is a representative LOWESS (locally weighted scatterplot smoothening) curve for the scatter. The LOWESS curve can be analyzed by dividing it into four segments (I, II, III and IV). In segment I, a sudden increase in number of clusters occurs with slight decrease in inconsistency coefficient. It is because each cut-off at top levels of binary joints results in higher number of

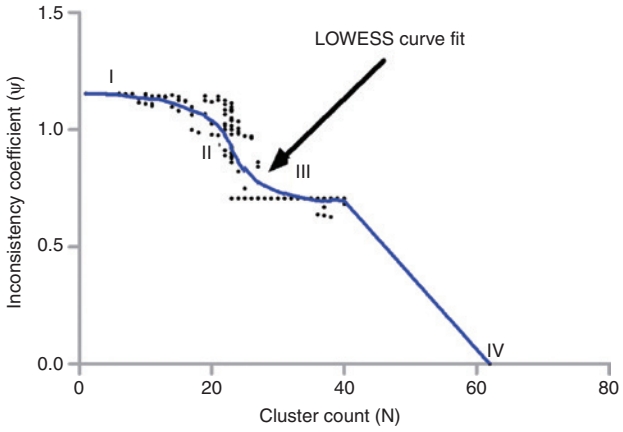

Figure 9: LOWESS curve fit and different segments ($Vf = 0.1$).

isolated clusters. Segment II shows an opposite behavior where the reduced inconsistency coefficient does not affect the number of clusters much. This is the stage when the object (fiber) dedicates itself to a single cluster rather than getting isolated and hence shifting between clusters. Segment III is represented by the portion of curve that asymptotes to $\Psi = 0.7071$. A sudden surge in cluster count is noticed when clusters are further subdivided and objects per clusters gets reduced to 2 ~ 3. It is indicative of a sample reaching its percolation threshold that indicates the presence of a connected path of fibers from top to bottom of the sample below this index. There is no connection above this level. Therefore, $\Psi = 0.7071$ has been chosen to compare clustering strength for different volume fractions. Corresponding numbers of clusters are taken from the LOWESS fit curve. Point IV belongs to the inconsistency coefficient = 0. Here each object is a potential cluster in itself, and cluster count is equal to the number of objects. Figures 10 and 11 indicate the advancement of clustering by reducing the hierarchical inconsistency coefficient from $N = 1$ for $\Psi = \Psi_{max}$ to $N = N_{max}$ for $\Psi = 0$. Here N_{max} is the number of objects.

3 Metric development and normalization

The metric to geometric characterization of any fiber matrix architecture is developed from the inconsistency coefficient (Ψ). Normalization is done to remove the dependence on fiber volume fraction. Several studies have been taken up in the past to evaluate the clustering score of different types of architecture through normalization of nearest-neighbor distance [12–14]. In this work

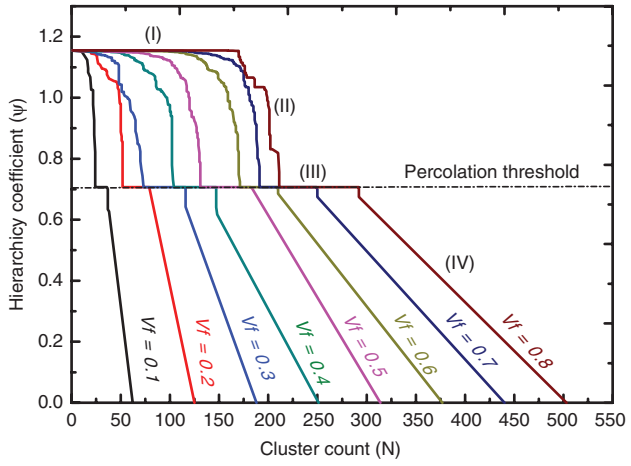

Figure 10: Plot between cluster count (N) generated vs. inconsistency coefficient (Ψ) for different volume fractions (*vf*).

clustering is dependent on twin parameters of cluster count and their individual strength, and it is described in a manner that for the densest model of hexagonal arrangements its magnitude is maximum. The densest packing of fibers (Figure 12) is analogous to the hexagonal lattice of the bee's honeycomb [15] with a packing volume fraction of ≈0.9.

The graph shown in Figure 13 illustrates a linear relationship between the number of clusters and the volume fraction. It can be noticed that the number of clusters increases with the volume fraction. On a comparative scale a calibration measure is proposed as

$$N^{*}_{vf} = N_{vf\ (\Psi=\bar{\Psi})}\left\langle \frac{N_{vf\min\ (\Psi=0)}}{N_{vf\ (\Psi=0)}} \right\rangle. \tag{3}$$

This description eliminates the effect of the chosen clustering coefficient ($\bar{\Psi}$). Here $N_{vf\min}$ is the count of clusters corresponding to minimum volume fraction taken as reference on a comparative scale. N_{vf} is the cluster count for a particular volume fraction. It is desirable to normalize the volume fraction dependence during the clustering analysis so that the level of clustering of any arbitrary sample can be determined irrespective of its volume fraction.

If clustering score (η_{cl}) is chosen as the statistical descriptor of the clustering for hierarchical partitioning using corresponding to a chosen inconsistency coefficient, an equation of normalized form to approximate the clustering score is suggested as

$$\eta_{cl} = \left\{ N^{*}_{vf}\left(\frac{vf}{vf_{\text{normalizing}} - vf} \right) \right\}^{0.5}. \tag{4}$$

The normalization is done with respect to the highest volume fraction sample. Using the proposed Equation (4), it can be noticed that as *vf* approaches $vf_{\text{normalizing}}$, the clustering strength asymptotes to an indefinite value. Therefore, the bee's honeycomb model attains the highest strength. Substitute $vf_{\text{normalizing}} = vf_h$ (common threshold of fiber volume fraction) in Equation (4). The graph between statistical descriptor of clustering η_{cl} and *Vf* (Figure 14)

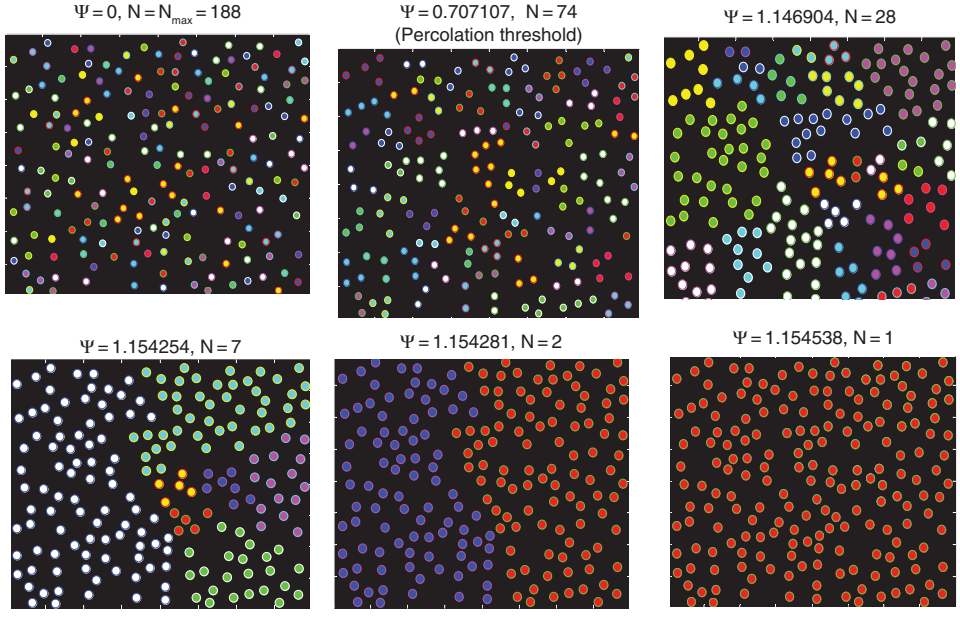

Figure 11: Progression of clustering with inconsistency coefficient for the range between highest and lowest values of inconsistency coefficient (Ψ) for a randomly seeded sample of *vf* = 0.3.

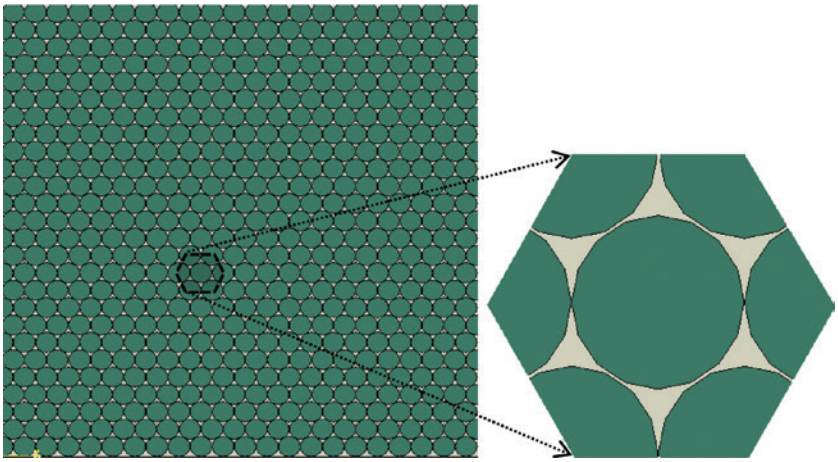

Figure 12: Hexagonal model of densest packing with maximum volume fraction $vf_h = \frac{1}{6}\pi\sqrt{3} \approx 0.9$.

indicates the linear increase of clustering strength for the initial volume fractions (0.1 ~ 0.7). A sudden rise in the clustering score is observed as volume fraction goes beyond 0.7. It asymptotes to ∞ for the peak fiber volume fraction ($vf_h = 0.9072$).

4 Transient moisture diffusion analysis

The way in which composite materials absorb moisture depends upon factors such as fiber volume fraction, reinforcement orientation, fiber nature (that is, permeability, polarity, density, etc.), area of exposed surfaces, diffusivity, and surface protection [16–19]. Therefore, any microstructure should consider at least one of these factors as the basis of concerned study. The current work studies the effect of fiber volume fraction (*Vf*). Some significant modeling done in this area include heat transfer, stress buildup, and interface failure studies [20–23]. To the author's knowledge there is not any prior research work that describes the effect of fiber volume fraction on geometric clustering and diffusion behavior.

4.1 Governing theory

Figure 15 represents the diffusion model chosen to predict the moisture ingress inside a typical FRP along the cross-section. The initial moisture concentration C_i inside the two-dimensional domain is uniform. The sudden exposure to moisture boundary condition results

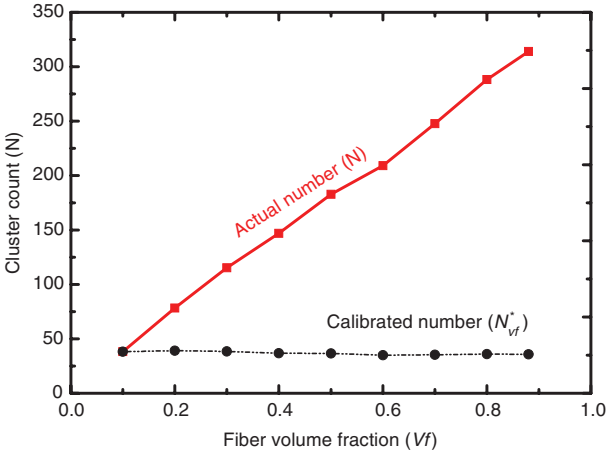

Figure 13: Cluster count vs. volume fraction graph for randomly packed arbitrary samples taken at percolation threshold ($\Psi = \bar{\Psi} = 0.7071$) and calibration curve post normalization (N^*_{vf}).

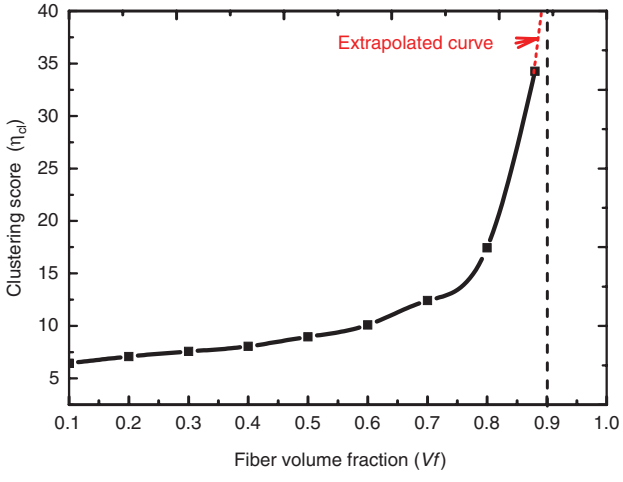

Figure 14: Volume fraction vs. final clustering score and asymptote line representing the indeterminable clustering score for densest packing.

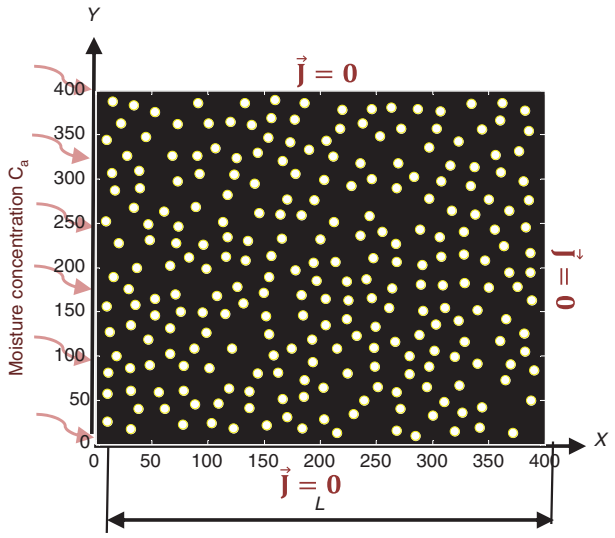

Figure 15: Representation of moisture diffusion through FRPs.

in concentration over left face reaching instantaneously the ambient moisture concentration C_a. If D_m is the diffusivity of material, the mass diffusion behavior is described by Fick's second law with the governing equation of the form

$$\frac{\partial c}{\partial t} = D_m \frac{\partial^2 c}{\partial x^2}. \tag{5}$$

The periodic boundary conditions have been applied by assuming an infinitely long lamina in the X-direction. The RVEs are periodically repeating along the X-direction and symmetric about the Y-direction. Initially (at time t = 0) the entire RVE is assumed to have no moisture content, i.e.

$$C = 0 \ (\Omega, \ \forall t = 0). \tag{6}$$

An instantaneous exposure of the left edge from the dry state to the ambient environmental moisture (C_{amb}) results in the mass diffusion inside the RVE. The boundary conditions for moisture exposed left edge are

$$C = C_{\text{amb}} \ (x = 0, \forall t > 0). \tag{7}$$

The ambient moisture is maintained throughout the diffusion simulation. In Figure 15 the rest of the three edges are assumed to be impermeable boundaries with no moisture flux ($\vec{J}$) either entering or leaving them for the entire duration; the boundary conditions of these edges are

$$\vec{J} = 0 \ \ (x = a, y = 0, y = b, \forall t \geq 0) \tag{8}$$

Fick's second law is used to find concentration at any given time instance $C(t)$ [24]

$$\frac{c(t) - c_i}{c_a - c_i} = 1 - \frac{4}{\Pi} \sum_{j=0}^{n} \frac{1}{(2j+1)} \sin \frac{(2j+1)\Pi x}{L} e^{\left[\frac{D_m (2j+1)^2 \Pi^2 t}{L^2}\right]}. \tag{9}$$

4.2 Microstructure generation

The microstructures representing random arrangement of fibers within a square lamina were generated with variable fiber volume fraction. An in-house computational code was written for the artificial microstructure generation. The circular fibers having diameter (d) at different volume fractions were placed by choosing random coordinates. The densest microstructure with *Vf* ~0.88 contained approximately 450 circular reinforcements each of 18 μm diameter size within a square window of size 0.16 mm^2. The first algorithm to create models of *Vf* up to 0.5 is fairly simple; it can randomly seed a given area with fibers. The compatibility check was employed to prevent an overlap with any pre-existing reinforcements. The algorithm can seed fairly faster for the *Vf* up to 0.55. It required special heuristics to generate *vf*'s beyond 0.55. It was done by the moving the existing seeds closer and generating some free space for the new seeds.

4.3 Finite element analysis

The finite element analysis was conducted on the commercial finite element code ABAQUS [25]. The moisture content is specified as the nodal unknown in the diffusion analysis. In the current problem the moisture transports into the model through the left boundary which is exposed to the moisture environment. Hence, the environmental moisture content is specified as the moisture boundary condition on the left edge. There is no initial moisture content. All the models were meshed using four-noded convective/diffusive quadrilateral element (DCC2D4). Since the microstructures were homogeneous, all the microstructures were finely meshed with approximately 12,000 elements for each model. The mesh convergence was studied to ensure that the size of elements is fine enough to give close results from the numerical viewpoint. The properties of fibers and matrix used in the analysis were taken from [20, 21]. The moisture and boundary conditions are taken from experimental works by [20]. The diffusivity of the matrix is 54.4×10^{-14} m^2/s, and boundary moisture is 1.48% (w/w). Figure 16 illustrates

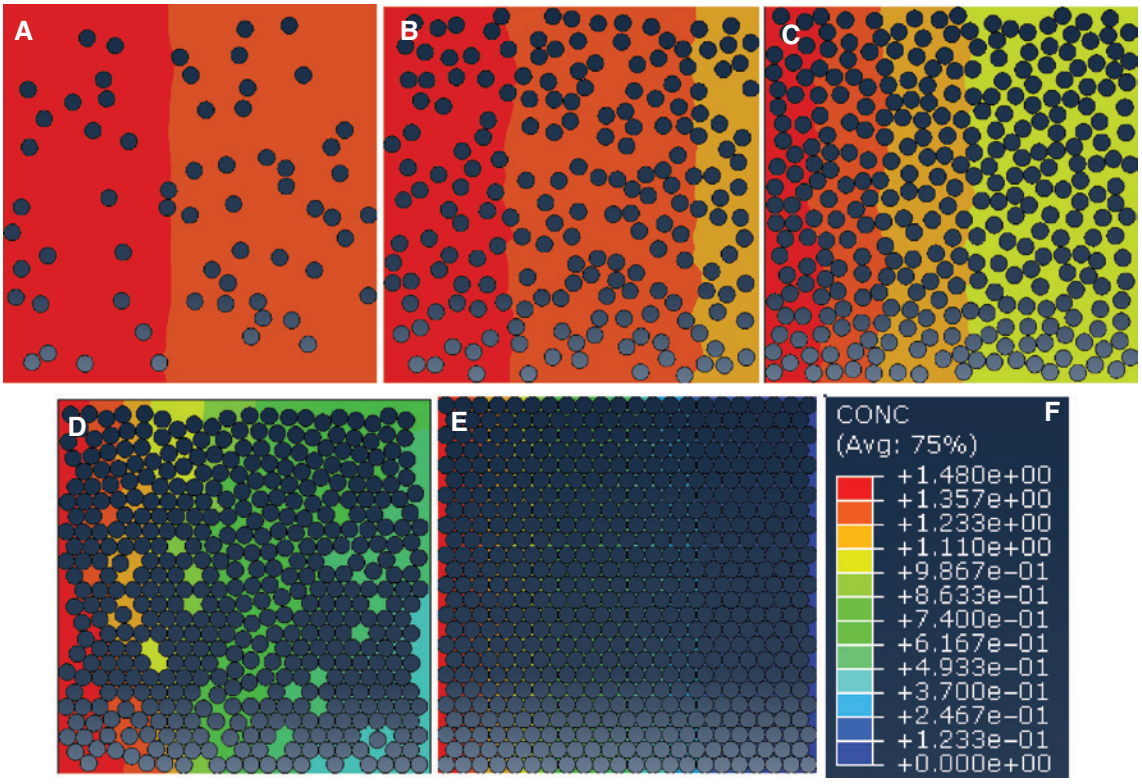

Figure 16: Moisture distribution profiles at different time intervals at (A) 0.1, (B) 0.3, (C) 0.5, (D) 0.7 and (E) 0.88 fiber volume fractions.

the moisture distribution within the different microstructures. The fibers are hydrophobic in nature, and moisture diffuses only through the matrix. Therefore, the presence of fibers enhances the moisture barrier characteristics of the composite.

The finite element simulations were carried out for various volume fractions (0.1–0.88). Fickian diffusion model is used. In order to interpret the evolution of moisture, the fraction of saturated epoxy was measured along with the progression of the moisture. The moisture saturated epoxy is the region where moisture equals the boundary moisture. Commercially available software Image J is used for color calibration and to measure the area. This is illustrated by the example in Figure 17. In this figure, the area fraction of saturated epoxy is almost 12.8 percentile of the model area or approximately 16 percentile of the matrix area (considering matrix occupies 80% of total representative volume at $Vf = 0.2$) at time $t = 90{,}000$ s.

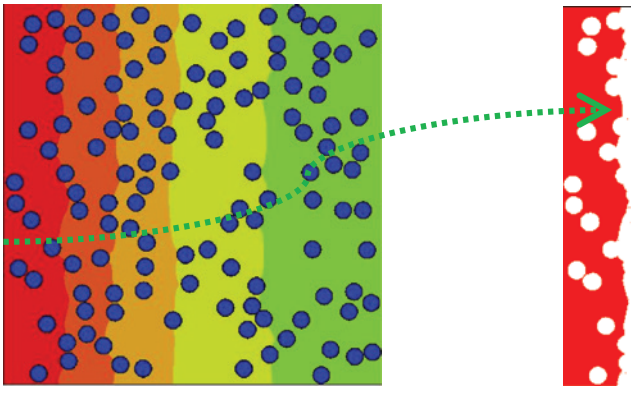

Figure 17: Image extraction to compute area fraction at a given time instance.

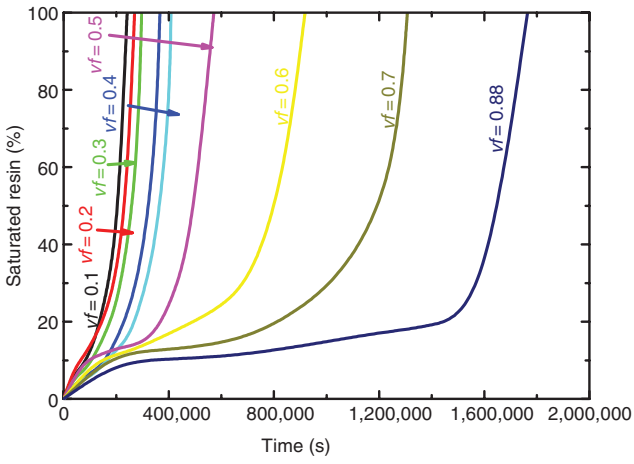

Figure 18: Fraction of saturated epoxy phase at different time points for different volume fractions.

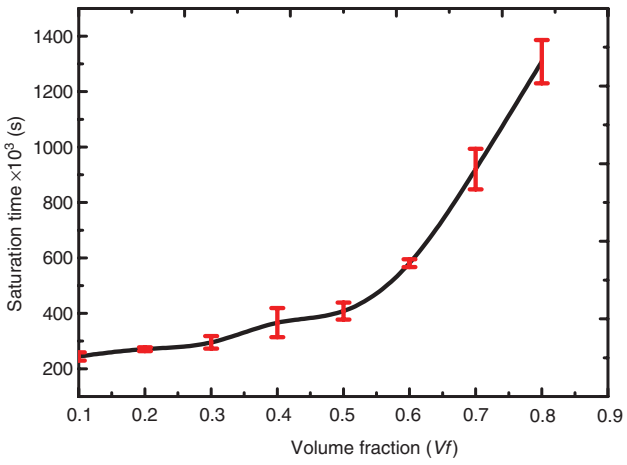

Figure 19: Volume fraction vs. saturation time.

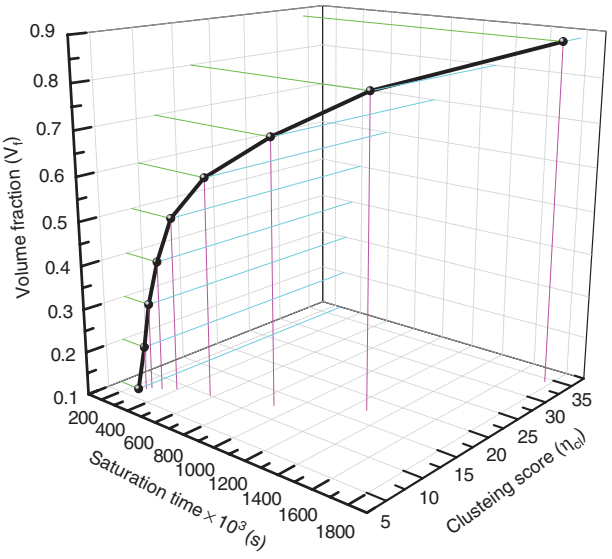

Figure 20: Saturation duration and clustering scores across volume fractions.

Figure 18 shows the fraction of saturated area measured at different time steps for different fiber volume fractions. Four different microstructures are evaluated for each volume fraction in order to get a statistically averaged saturation time response. Hence, 32 different microstructures were simulated for eight different fiber volume fractions.

Figure 19 shows the time taken for the saturation of the matrix phase at different volume fractions. The error bars show the maximum and minimum values of saturation time observed for the microstructures that have the same volume fraction. A few important observations can be made based on this plot. The curves remain comparatively flat for *Vf* up to 0.3. This behavior can be attributed to the presence of resin dominated regions that facilitate the moisture transport. With an increase in volume fraction the fiber dominated clustering plays an important role. Any increase in fiber content beyond a volume fraction (*Vf*) of 0.3 results in the reduced rate of mass transport. It results in a higher saturation time. Increase in *Vf* beyond 0.6 has a dramatic effect on the moisture transport behavior, and progression of moisture slows down significantly. Figure 20 is a 3-D plot that reports all three parameters simultaneously. It can be noticed that the proposed metrics based on cluster count can effectively describe the clustering score and give an approximate diffusion response for any given fiber volume fractions for two-phase FRP composites.

5 Conclusions

The paper describes a novel statistical approach to craft the clustering metrics and estimate the diffusion response inside clustered FRPs. The method of hierarchical clustering is used to develop the geometric descriptor of clustering inforced polymer composites for its geometric characterization. Two-step normalization is adopted to reduce the effect of volume fraction on clustering descriptor. The proposed descriptor shows a good correlation with the saturation time across the volume fraction. The present approach can help in quick evaluation of the moisture transport characteristics for a given microstructure of two-phase reinforced polymer composites with an arbitrary shape and volume fraction.

Appendix

A Usage of inconsistency coefficient to create natural divisions – an example

Figure 21 represents two-dimensional domain with five data points. In the context of the current problem these points can be regarded as fibers within the matrix. The dendrogram shows a hierarchical cluster tree. Inconsistency coefficient for each link is indicated in cluster tree that is calculated from Equation (1).

Executing the in-house algorithm in MATLAB environment [26] resulted in the identification of clusters (Figure 22). The figure shows the variation in the number of clusters with the change in the inconsistency coefficient (Ψ).

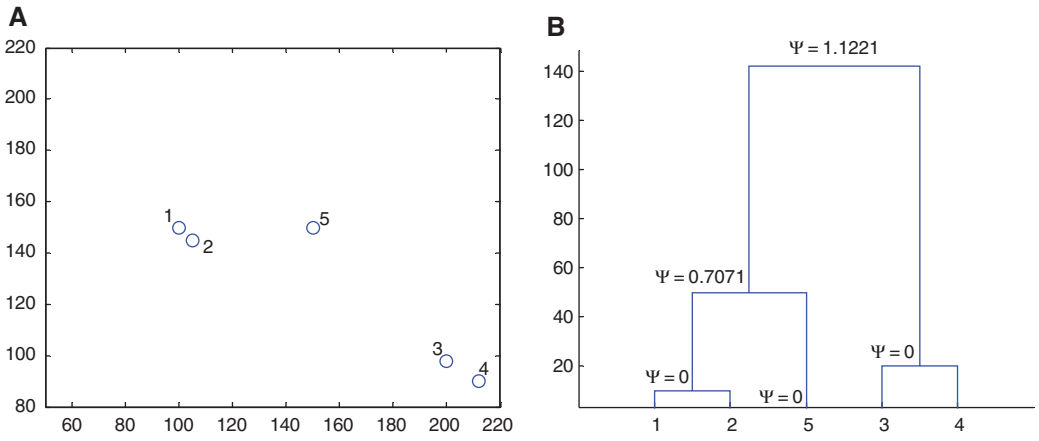

Figure 21: Hierarchical clustering illustration of (A) sample and (B) dendrogram representing binary joints and inconsistency coefficient at each joint level.

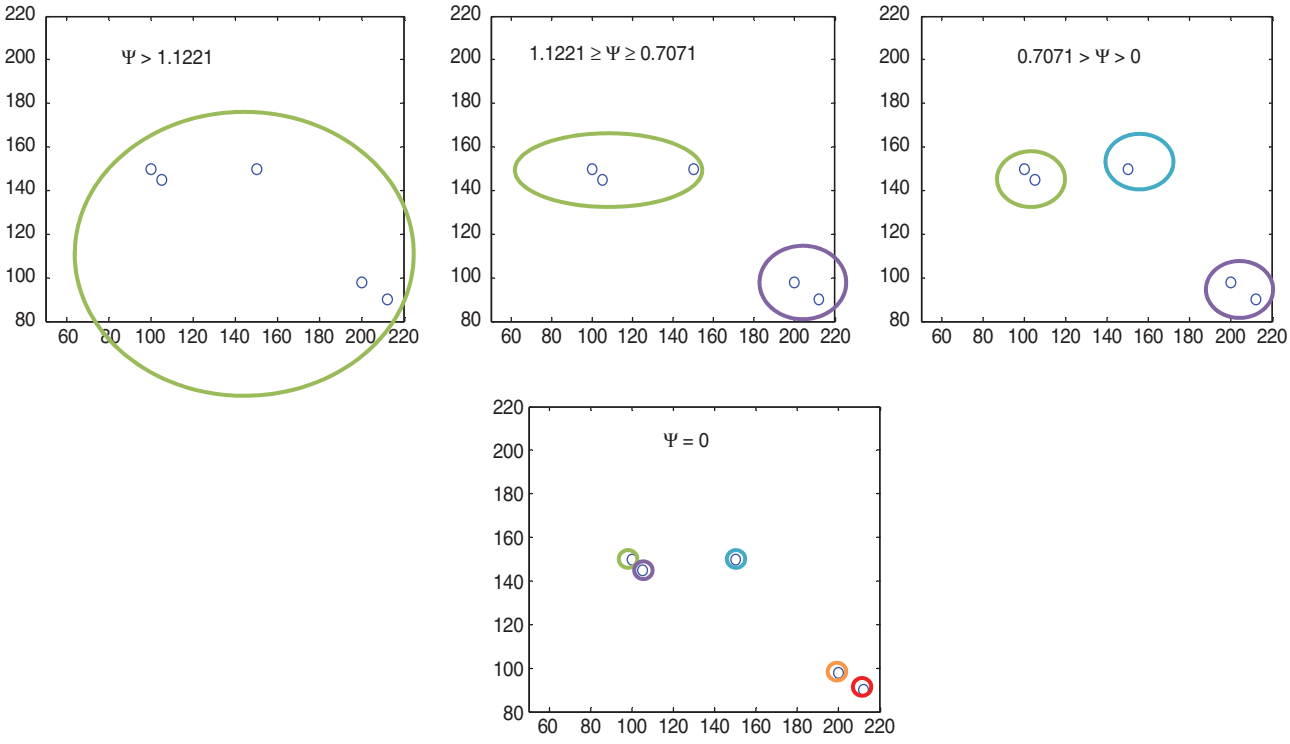

Figure 22: Hierarchical clustering progression on reducing the inconsistency coefficient (Ψ).

References

[1] Ezrin M, *Plastics Failure Guide: Cause and Prevention*, Hanser Pub.: Munich, Germany, ISBN: 1569901848, 1996; 325.

[2] De Morais WA, D'Almeida JRM, Godefroid LB. *J. Braz. Soc. Mech. Sci. Eng*. 2003, 25, 325.

[3] Raghavan P, Li S, Ghosh S. *Finite Elem. Anal. Des*. 2004, 40, 1619–1640.

[4] Sevostianov I, Kushch V. *Int. J. Solids Struct*. 2009, 46, 4419–4429.

[5] Vaughan TJ, McCarthy CT. *Compos. Sci. Technol*. 2011, 71, 388–396.

[6] Bond DA. *J. Compos. Mater*. 2005, 39, 2113.

[7] Boukhoulda BF, Adda-Bedia E, Madani K. *Compos Struct*. 2006, 74, 406–418.

[8] Jain D, Mukherjee A, Kwatra N. *Appl. Math. Model*. 2016, 40, 1873–1886.

[9] Ramamurty U, Seshacharyulu T. *Mater. Sci. Eng*. 1999, 268, 97–103.

[10] Trias D, Costa J, Turon A, Hurtado JE. *Acta Mater*. 2006, 54, 3471–3484.

[11] Swaminathan S, Ghosh S, Pagano NJ. *J. Compo. Mater*. 2006, 40, 583–604.
[12] Wilding SE, Fullwood DT. *Comput. Mater. Sci*. 2011, 50, 2262–22672.
[13] Segurado J, Gonzalez C, Llorca J. *Acta Mater*. 2003, 51, 2355–2369.
[14] Li M, Ghosh S, Richmond O, Weiland H, Rouns TN. *Mater. Sci. Eng*. 1999, A265, 153–173.
[15] Steinhaus H. *Mathematical Snapshots*, 3rd ed., Dover: New York, 1999, p. 202.
[16] Thomason JL. *Composites* 1995, 26, 467–475.
[17] Thomason JL. *Composites* 1995, 26, 477–485.
[18] Jain D, Mukherjee A, Kwatra N. *Int. J. Heat Mass Transf*. 2014, 76, 199–209.
[19] Thomason JL. *Composites* 1995, 26, 487–498.
[20] Vaddadi P, Nakamura T, Singh RP. *Acta Mater*. 2003, 51, 177–193.
[21] Vaddadi P, Nakamura T, Singh RP. *Compos. Part A Appl. Sci. Manuf*. 2003, 34, 719–730.
[22] Loh W, Crocombe A, Abdel Wahab M, Ashcroft I. *J. Adhes*. 2003, 79, 1135–1160.
[23] Jain D, Mukherjee A, Kwatra N. *Int. J. Heat Mass Transf*. 2015, 86, 787–795.
[24] Jost W. *Diffusion in Solids, Liquids, Gases*, Academic Press: New York, 1960.
[25] ABAQUS/STANDARD 6.13; 2014. <http://www.simulia.com>.
[26] MATLAB 7.13; 2011. <http://www.mathworks.com>.